Coronal Solar Magnetism Observatory
Technical Note 4, Rev 0

An Analysis of Scattered Light in Reflecting and Refracting Primary Objectives for Coronagraphs

Peter G. Nelson

ABSTRACT:

To observe magnetic fields in the solar corona, very low levels of instrumental background are required. The primary contributor to instrumental background light in an internally-occulted coronagraph is light scattered from the primary lens or mirror. This is caused by surface roughness, particulate contamination, and (in the case of refractors) imperfections of the glass. To obtain good coronal data, the scattered light intensity in the coronal image should be less than or on the order of the coronal brightness (a few ppm of the disk center). We examine the sources of scattering and estimate the level of scattering from each for both reflectors and refractors. We conclude that refractors have a significant advantage over reflectors for the dominant sources of scattered light.

Modeling Scattering

There are two types of scatterers: distributed and local. Distributed scattering mechanisms are uniform over a surface, and the scattering has a translational invariance. Examples are microroughness and disordered arrays of discrete scatterers (dust). It is assumed in scattering theory that linear superposition applies, and therefore non-local scattering only depends on the total power incident on the scattering surface and not the incident intensity (for example, twice the power over half the area produces the same scattering). Distributed scattering is described by the Bi-directional Scattering Distribution Function, or BSDF:

$$BSDF = \frac{dP}{d\omega\, P_i\, \cos(\theta_s)} \qquad \left[sr^{-1}\right] \qquad [1]$$

where dP is the differential power scattered into the solid angle $d\omega$ centered about a polar angle θ_s from the surface normal. P_i is the total incident power. The $\cos(\theta_s)$ term corrects for the reduced (projected) scattering area seen by the observer; at low angles the BSDF has to be larger to produce the same $dP/d\omega$. Note the BSDF is not a function of

the scattering surface's area, but will depend on the polar angles for both the incident and reflected (or transmitted) light. The BSDF is also known as BTDF (Bi-directional Transmittance Distribution Function) or BRDF (Bi-Directional Reflectance Distribution Function) for transmitted and reflected scattering respectively. Most of this report centers on evaluating the relative BSDF for the two cases of a reflecting and refracting coronagraph objective.

The second class of scatterers describes isolated point defects. Relevant examples are singular dust particles or air bubbles in the glass of a lens. Unlike distributed scatterers, the scattering from point defects depends on the incident light *intensity* (W/m^2). They are described by the Differential Scattering Cross Section, or DSC:

$$DSC = \frac{dP}{d\omega\, I_i} \qquad \left[m^2 sr^{-1}\right] \qquad [2]$$

where I_i is the incident intensity. Note that the units for the DSC are different from the BSDF. The $\cos(\theta_s)$ term is also absent, since there is no 'projected surface area' for scattering from a point-like particle or defect. Like the BSDF, the DSC is a function of the incident and scattered polar angles. We will evaluate the DSC for spherical air bubbles in the glass and for dust particles.

In all the calculations, the incident angle is approximately zero ($\cos(\theta_s)\approx 1$), and the scattered light is azimuthally symmetric so the BSDF and DSC will only be a function of the scattering angle (θ_s).

What is the scattering angle (θ_s) for a solar telescope? The definition for the BSDF and DSC are defined for scattering from flat surfaces. Consider a small sub-aperture on the optical axis of a refracting telescope. On the optical axis, the lens does not bend light (the front and rear lens surfaces are locally parallel), and the telescope essentially becomes a pin-hole camera with a piece of glass over the hole which will scatter light (Figure 1 below).

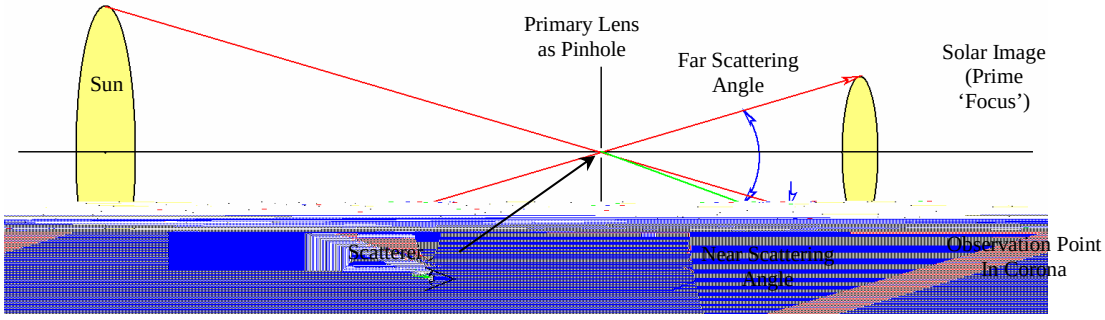

Figure 1: Understanding the scattering angle in the 'pinhole' limit

If we assume that the light from any point on the sun is parallel as it is incident on the pinhole, then this looks exactly like the classic scatterometer setup; every point on the sun has a well defined incidence angle with the scattering surface (the pinhole), and a well-defined scattering angle to the detector at the Observation Point (OP) in the corona.

Fortunately, polished glass surfaces have a property called *shift invariance* which says the scattering is only a function of the *difference* in the angle between the scattered and the specular light. In our calculations, we assume an incident angle of zero, and calculate the scattering over the range of scattering angles shown in blue in Figure 1. The angle ranges from 0.0025 to 0.55 degrees at an observation point $0.01R_\odot$ from the limb. If the coronagraph has a 1 degree FOV, then the largest scattering angle is 0.75 degrees.

For any other sub-aperture of the lens, roughness or particulates on the front surface can be thought of as a scatterer plus a 'perfect' prism which deflects both the specular and the scattered light. All sub-apertures form coincident solar images, and thus are identical. Indeed, we would expect all sub-apertures to produce images of equal quality. This allows us to use the flat-surface BSDF and DSC to describe a system without considering the focusing properties of the lens. Similar arguments can be made for a mirror or the back surface of a lens. For a lens, the total BSDF is obtained by multiplying the scattering calculated for the front surface by a factor of 2 (this assumes equal polish quality and contamination on both the front and back surfaces of the lens).

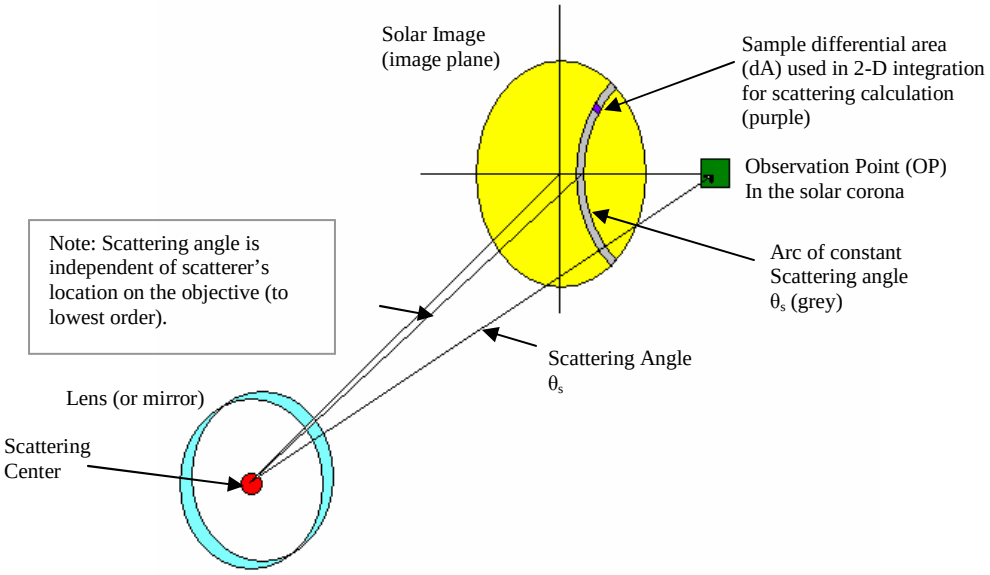

Figure 2: 3-D illustration of the lens, solar image, and scattering angle

The main tool used for calculating BSDFs in this report is the Modeled Integrated Scatter Tool (MIST - v.2.10) developed by Dr. Thomas A. Germer at the Optical Technology Division of the National Institute of Standards and Technology in Gaithersberg, MD. The software is capable of evaluating both reflected and transmitted scattering using all of the most common models for both scatterers and substrates. This includes modeling transmission through substrates with $n \neq 1$. It is available license-free at the NIST web site. We do not use ray-trace or monte-carlo modeling (ASAP, Zemax, Code-V, etc.) to evaluate scattering as others have done[1]. Such modeling is important when considering light scattered from telescope structures (struts, lens cells, etc.), domes, and other objects, but has no significant advantages when comparing scattering caused at the surface of telescope primaries. Historically, structural scattering has not been a dominant factor

(shown later) and it is assumed that it can be controlled to equal levels in both refracting and reflecting designs.

We assume a wavelength (λ) of 1074nm in our modeling. This corresponds to the Fe XIII coronal emission line which has a high figure of merit for magnetic field measurements and is not contaminated by terrestrial atmospheric lines.

Limitations of Scattering Models

It is very important to note that scattering models depend on the exact nature of the scatterers. The results presented here are based on simple power-law models of microroughness, and dust is modeled as distributions of spherical scatterers (Mie scattering). It is certain that pollen, animal hair, bugs, and other components of real-world detritus are not well described by these models. Though this study tries to estimate the levels of scattered light, the calculations are inherently limited. Despite this, the modeling should work quite well for comparing the relative merits of refracting vs reflecting designs. Though animal hair is not well described by a sphere, it is difficult to imagine a particulate contaminant which scales differently in refractors and reflectors than a sphere does.

A major limitation in comparing reflectors and refractors is the uncertainty associated with the scattering properties of aluminum coatings. This has turned out to be very difficult to evaluate. Most low-loss, low-scattering mirror studies are conducted on dielectric mirrors. The scattering properties of aluminized surfaces will be presented in detail.

There are also problems in the specification for microroughness. Most manufacturers use "RMS surface roughness" to describe surface finish. Unfortunately, this is inadequate to describe a real surface. A large number of polished surfaces (and particularly glass) are 'fractal' in character; a 2-D PSD of the surface has a characteristic and constant slope at all spatial frequencies. Though this slope is very consistent for glass, it does vary to some extent. Different polishing techniques may produce different slopes. As a result, two surfaces with the same RMS specification may have very different roughness at any given spatial frequency. Slope issues aside, all surface roughness measurement techniques (Total Integrated Scatter (TIS), AFM profilometers, interferograms) have different inherent bandwidths. To accurately specify an RMS value, the bandwidth should be specified (and it usually isn't).

It is also not uncommon for the scattering from real surfaces to differ from theoretical values, as "non-topographic" sources of scatter are often present (such as spatial fluctuations in the optical constant of a coating due to grain boundaries, etc.). In this study, we make extensive use of "wavelength scaling" to compare BSDFs made at different wavelengths, and assume the only difference between a "1-D" and a "2-D" power spectrum (see below) is a simple change in the power law. Stover[2] notes that both of these assumptions are model dependent and Germer[11] points out that aluminum is known to not scale very well with wavelength. In particular, the conversion between 1-D and 2-D PSDs is 'a tricky subject.' Although polished glass substrates and deposited aluminum coatings satisfy the basic requirements for the 1-D to 2-D PSD conversions we

use, we did not investigate the validity of "wavelength scaling" for deposited aluminum coatings. The scattering data we found were difficult to compare for many reasons, and wavelength scaling probably contributed to this.

Evidence presented here and elsewhere[1] suggests that scattering in coronagraphs is dominated by environmentally-derived contamination of the primary's surface. Characterizing contamination at different sites is virtually impossible as it depends in great detail on the telescope and dome structure, the time of year, weather, etc.

Scattering due to Microroughness

The quality of isotropic 2-D surfaces is often determined by sampling the height along a randomly selected line across the surface (with an AFM, optical profilometer, or other instrument). A 1-D power spectral density (PSD) in microns[3] (microns[2] per unit spatial frequency in microns[-1]) is calculated from these data. There are several ways to parameterize the roughness of surfaces. The ABC model (also known as the K-correlation model) is a common parameterization:

$$S_2(f) = \frac{A_2}{\left[1 + (B\ f)^2\right]^{(C+1)/2}} \qquad [3]$$

The subscript (2) refers to the fact that this is a model for a 2-D power spectrum, following the convention in Stover[4]. The 1-D spectrum has the same form, except the power in the denominator is (C/2); the slope of the 2-D spectrum is one power of frequency steeper than the 1-D spectrum of the same surface, at high spatial frequencies. In Stover's convention, (C) is the slope of the 1-D PSD. (A_2) gives an overall scaling and (B) describes at what frequency below which the power law becomes flat. If these parameters can be determined (and the 1-D slope C is greater than 1), then the RMS roughness (σ) is readily calculated:

$$\sigma = \left[2\,\pi \int_0^\infty S_2(f)\ f\ df \right]^{1/2} \qquad [4a]$$

$$A_2 = \frac{B^2\ (C-1)\,\sigma^2}{2\,\pi} \quad \text{or} \quad \sigma = \sqrt{\frac{2\ A_2\ \pi}{B^2 (C-1)}} \qquad [4b]$$

If C is ≤ 1, the integral doesn't converge. In such instances, the integral must be calculated over a limited band (evaluating the integral to infinite frequency isn't physical in any case). The Laser Interferometer Gravitational Wave Observatory (LIGO) project has applied 'super polish' finishes to ø250x100mm fused-silica substrates and measured[3] their surface roughness (a sample shown in Figure 3) down to 0.1cm^{-1}.

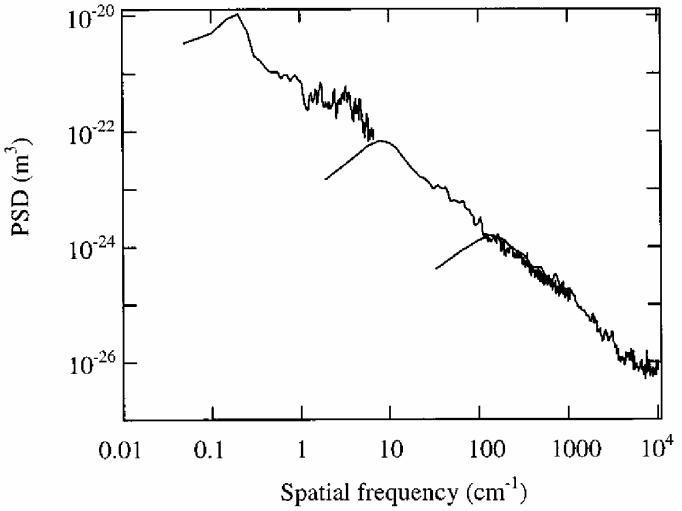

Figure 3: The PSD of an uncoated polished fused silica substrate from LIGO

Stover[4] shows that there is a direct correlation between the PSD (as in Figure 3) and the BSDF. If one converts the horizontal scale from microns^{-1} to angle using the grating equation:

$$\sin(\theta) - \sin(\theta_0) = n \cdot f_{spatial} \cdot \lambda \qquad [5]$$

the BSDF amplitude is proportional to the 2-D PSD. Note that in the lowest order (n=1), the scattering into our field of view (0.0025 to 0.75 degrees) corresponds to spatial frequencies with characteristic lengths of ~0.08mm to 2.5cm! The term 'microroughness' would seem to be a bit of a misnomer, since scattering at these low angles is really caused by errors in the figure more than the micro-scratches that one associates with 'microroughness'.

The parameterization in Equations [3] and [4] is unfortunate because the factor (B) is so dominant, yet there's no clear evidence of a low-frequency roll-off in Figure 3 or any other reference we've found. (B) is also irrelevant in that the spatial frequencies affecting the coronagraph are above the limits for (B) these data suggest. Since (B) is not easily determined from data, the relationships in Equation [4b] should be avoided for making estimates of BSDFs or calculating RMS roughness values. The RMS value for Figure 3 was calculated in two different frequency bands by the authors ("0" - 4.3cm^{-1} and 4.3 – 7500cm^{-1}), and found to be 0.5 and 0.4 nm respectively.

Despite practical issues in the calculation of RMS roughness, Equation [4b] does tell us how the amplitude of the PSD will scale with the RMS roughness: the amplitude (A_2) scales like the RMS value squared. Since the BSDF is proportional to (A_2), the total scattering increases quickly with increasing surface roughness σ. An example of this dependence is given below.

Ball-park estimates of the RMS roughness limits can be had if one assumes the scattering is Lambertian (light scattered uniformly in all directions). By calculating the maximum allowable $dP/d\omega$ in your FOV, and multiplying by 2π, you get the Total Integrated Scatter (TIS). TIS has a simple relationship to the RMS roughness of a surface[5]:

$$TIS(\textit{in reflection}) = \left(\frac{4\pi\sigma}{\lambda}\right)^2 \qquad [6a]$$

$$TIS(\textit{in transmission}) = \left(\frac{2\pi\sigma}{\lambda}(n-1)\right)^2 \qquad [6b]$$

where both expressions assume normal incidence ($\theta_i = 0$) for the specular beam, and (n) is the index of refraction of the glass in [6b]. Behind these relationships is an integration from 0 to ∞ in the calculation of σ, and the same caveats on bandwidth and the slope (C) apply here. It is interesting to note that for a given RMS surface roughness, the single-surface scattered light is 20 times lower in the transmitting optic(assuming n=1.45 for fused silica at 1074nm). Even considering a factor of two for the front and back surfaces of the lens, the scattering in a lens is still an order of magnitude better. Said another way, the RMS roughness requirement is three times less stringent for the transmitting optic than the reflecting one.

Unfortunately, this is an oversimplification since scattering from dust and roughness is *not* Lambertian. In fact, the scattering is strongly peaked in the forward direction and that peak is dominant within the 0.75 degree scattering angle that affects coronagraphs. The above example strongly suggests that transmitting optics might be significantly better when real BSDFs are considered.

To use the MIST software with the ABC model, we need to find values of (A_2), (B), and (C) which accurately describe the surface. (B) is only constrained to be above 10^4, but is otherwise arbitrary. To this end, we fix $B=10^5$, and find values for (A_2) and (C) which accurately represent the data in Figure 3 over the spatial frequencies from about 1-1000cm^{-1}. (C) can be directly read from the 1-D PSD slope, and we set it to 1.3. Other sources[3,6,7,19] have measured the 1-D PSD of fused silica with almost exactly the same slope. Germer has observed[11] that most polished surfaces have 1-D PSD slope between 1 and 1.5, so these data are comfortably within the standard range. Likewise, (A_1) can be determined from the data by simple fitting. Stover shows that A_1 and A_2 (the 1-D and 2-D scaling factors) are related by:

$$A_2 = A_1 \frac{B\,\Gamma[(C+1)/2]}{2\sqrt{\pi}\,\Gamma(c/2)} \qquad [7]$$

where A_2 is the 2-D scale factor needed by MIST, and Γ is the standard gamma function. By fitting, we find $A_1 \approx 0.016$, and therefore $A_2 \approx 300$. Putting these parameters in MIST generates the BSDFs shown in Figure 4.

Figure 4 confirms the earlier comparison of the TIS for reflecting and refracting surfaces; the refracting optic has an order of magnitude lower level of scattering, even when two surfaces are considered (a peak value of 7,600 in the BRDF vs 750 in the BTDF).

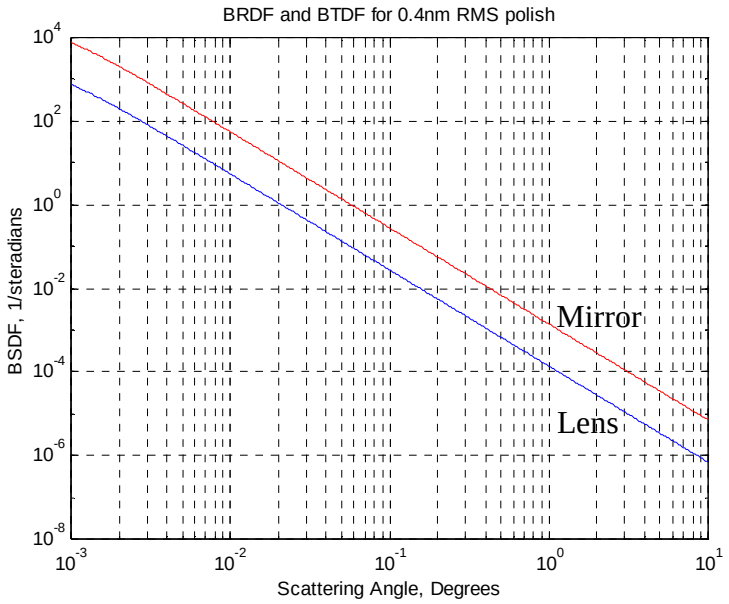

Figure 4: Expected BRDF and BTDF for LIGO-quality mirrors assuming the substrate microroughness perfectly 'prints through' the aluminized mirror coating.

Scattering Contribution from Aluminum Coatings

Unfortunately, the picture is not as simple as that shown in Figure 4. The aluminum coating deposited on the glass substrate has its own inherent scattering characteristics which are independent of the underlying substrate. John Evans in the early 60s noted:

> 'In the reflection coronagraph the pinholes, minute hills, and granular structure that appear in metals deposited on glass scatter more radiation than the imperfections within the glass of the ordinary system.' [8]

This should not be surprising. The assumption that 1nm of substrate roughness perfectly 'prints through' to the surface of an Al coating which is several hundred nm thick is not only difficult to imagine, but it is without any experimental support. To make matters worse, the spatial frequencies of interest for microroughness extend down to centimeter length scales, which means that the Al coating must be uniform *to the nm level* over distances of *several cm* – a 10^7 difference in scales. This is equivalent to having a field of snow 0.5m thick and 10 kilometers on a side which is uniform in thickness to 1mm. One could argue that coating techniques have improved since Evan's time, but there have also been great advances in polishing techniques. In addition, there is a significant body of experimental data which demonstrates this assumption is invalid.

Hickman[9] has made detailed micrograph images of surfaces before and after coating and found that "There was no observable correlation between the location of the scatter sites before and after coating was performed on any of the optics." He further noted: "Much higher levels of scatter were observed from the coated optics than from the bare substrates. This indicates that, for low-scatter substrates, the coating is a significant source of scatter from the coated optic." Bennett[10] found that the polarization of

scattered light from coated surfaces did not match theoretical models, and suggested that the distribution of grain sizes and shapes in films had to be considered. Indeed, Germer[11] points out that polycrystalline materials naturally have grain boundaries as do amorphous materials. Associated with these grain boundaries are micro-variations in the local optical constants. These local changes cause phase differences from different points on the surface, and hence scatter. Bennett also found that annealing significantly affected the scattering from films, which is necessarily contrary to a perfect substrate print-though model.

The relationship between the roughness of the substrate and the scattering properties of the coating seems unclear. Hickman found that float-polished substrates produced significantly lower levels of scatter (after Al coating) than conventional "super-polishing", even though the super-polished surface had a lower RMS roughness. Conversely, Bennett found that scattering from their samples was "…unaffected by the choice of file material (silver or aluminum), substrate material (glass or fused quartz), cleaning method, and film preparation method (evaporation or sputtering)." Some of the most compelling evidence that the scattering from coatings is unrelated to substrate roughness comes from a simple comparison of large-angle scattering (a few degrees from specular) of aluminum coatings on different substrates.

Harvey[1] measured the scattering of an aluminized substrate of "average" optical quality and found that the BRDF 5.7º from specular was $2x10^{-3}$ 1/str at 515nm and 45 degree incident angle (Figure 5 below).

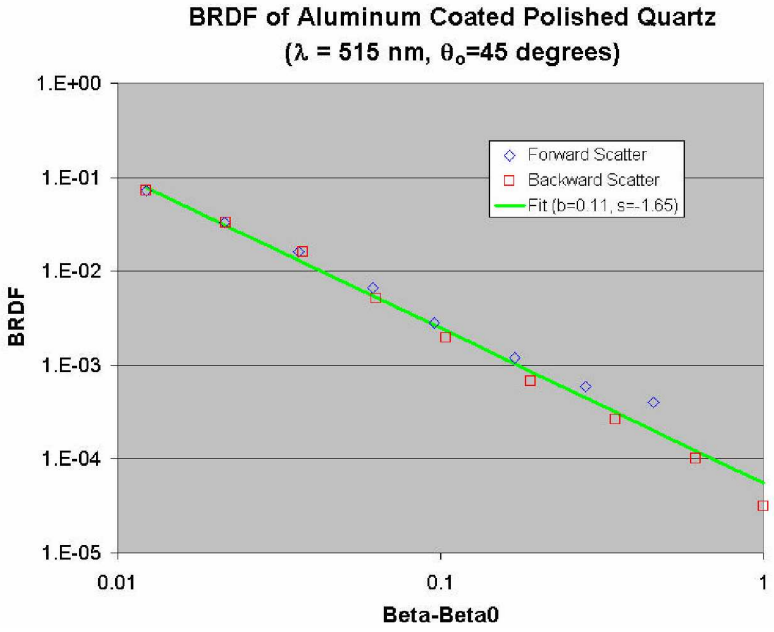

Figure 5: Direct measurement of BRDF for the Harvey mirror

Wang[12] made several measurements of a 70nm thick Al coating on a 0.8nm RMS super-polished fused silica substrate and found the BRDF at 5.7º to be $8x10^{-4}$ 1/str at 633nm and 10 degrees incident angle. Finally, Korendyke[13] measured one of the LASCO-C1 mirrors which had a 0.1nm RMS roughness and an AlSiO coating. Extrapolating his

measurements to 5.7º we find that at 633nm and 0 degrees incidence the BRDF was $3x10^{-4}$. Using MIST to scale all measurements to 0º and 1074, we find that the Harvey mirror was only a factor of two worse in scattering than Wang's mirror, and the LASCO-C1 mirror only a factor of two better than Wang. If Equations [4b] and [6a] are correct, and the 'print through' model valid, we would have expected the LASCO mirror to be 64 times lower in scattering than Wang's (scattering scaling like the roughness squared).

Even when the RMS roughness is measured after the coating is applied (using optical or stylus profilometers), the level of scattering is typically 4-9 times higher than Equation [6a] would predict. This is widely observed (see Wang, Hickman, Hyun-Ju,[14] Guenther,[15] and Kiesel.[16]) They all found that the large-area TIS measurements were dominated by point defects in the coating or low-level particulate contamination. Since stylus and optical profilometers typically 'miss' these defects, they underestimate the total scattering. Equation [5] accurately predicts the scattering when the TIS measurements were selectively made between defects. This is particularly bad news since it implies that even if the 'print through' model were correct, the level of scattering could be up to ten times higher than expected. The Korendyke, Hyun-Ju, and Duparré[17] have measured TIS as a function of position by reducing the area of the incident light to a very small beam. An example from Duparré is shown in Figure 6. The 'background' level between the peaks in this figure is consistent with the scatter level predicted by profilometers:

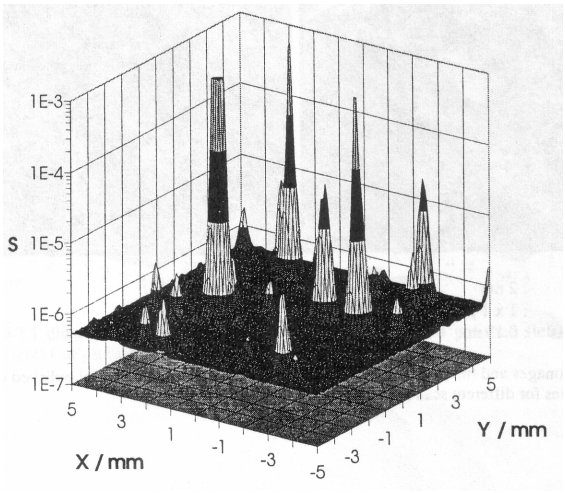

Figure 6: Position-resolved TIS measurements for a 0.06nm RMS polish on a Si wafer from Duparré. 'Point defects' not measured by profilometers dominate the scattering.

The most direct and convincing evidence we found for coating characteristics being unrelated to substrate roughness is that the slope of the measured BRDFs for aluminized surfaces differs significantly from the slope of the 2-D PSD for the substrates; these should match if a print-through model were correct. Gary Peterson of BRO has made many BRDF measurements of aluminized surfaces and claims that they always have a slope in the range of 1.5 to 1.8.[18] Germer has specialized in characterizing the roughness of *uncoated* surfaces and has observed that polished surfaces typically have 2-D PSD slopes in the range of 2.0 to 2.5.[11] Many references show the 2-D slope for super-

polished fused silica to be ~2.3.[3,6,7,19] Germer's BRDF measurements for uncoated surfaces have the same slopes as their 2-D PSDs and agree with standard scattering theory. Since the slope of substrate roughness is steeper than BRDF slopes, one might expect that the substrate roughness will dominate scattering (print through) at lower frequencies. Exactly this effect has been observed.

Duparré has measured the 2-D PSD of two surfaces, before and after depositing a 49-layer dielectric mirror coating (Al_2O_3/SiO_2)[17]. Those data are shown in Figure 7 below. The two surfaces were both fused silica and differed only by the level of polishing. The first sample was super-polished, and the second was polished with a standard RG1000 finish.

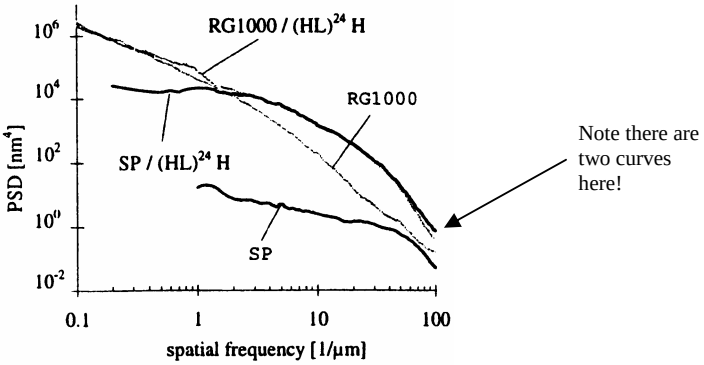

Figure 7: Print-though of surface roughness for a dielectric mirror.

The super-polished curves are shown in the heavy-weight lines and the RG1000 curves in the light-weight lines. For the super-polished sample, the post-coating PSD is much higher than the substrate roughness at all frequencies (print-through invalid). The RG1000 surface, on the other hand, is dominated by the coating above 0.2 μm^{-1} and by the substrate below. Though Duparré's dielectric coatings were significantly different than aluminum, this clearly illustrates the principle that 'print-through' can happen if the surface roughness exceeds the coating roughness.

The Two-Component Scattering Model for Coatings

Since there is evidence that the scattering from an aluminized surface is not (directly) related to its roughness, it makes sense to combine scattering due to substrate roughness and coatings directly in "BRDF space." This involves two assumptions: BRDFs calculated from substrate roughness using the standard theory is accurate if larger than the coating's contribution, and the measured BRDFs for Al can be extrapolated to lower angles. The first assumption seems reasonable, while Figure 5 shows that coating BRDFs have a very linear slope for two decades or more down to 0.5 degrees. Assuming the substrate print-through and coating contributions are uncorrelated, we can form a net BRDF by taking a quadrature sum of the two components.

The substrate surface roughness was described by the ABC as discussed earlier, with (C) set to 1.3, (B) set to $1x10^5$, and (A) is chosen to give a representative RMS roughness (1nm, 2nm, etc.). The bandwidth for the RMS calculation was 0.00043 to 100 μm^{-1}. This bandwidth was chosen to match reference [3], but modeling shows that the RMS

specification is only weakly sensitive to the chosen bandwidth. The A,B & C parameters were entered into MIST, and the BRDF was calculated at 1075nm assuming the optical constants of aluminum. This calculated BRDF was modeled as a simple power law for the scattering calculation.

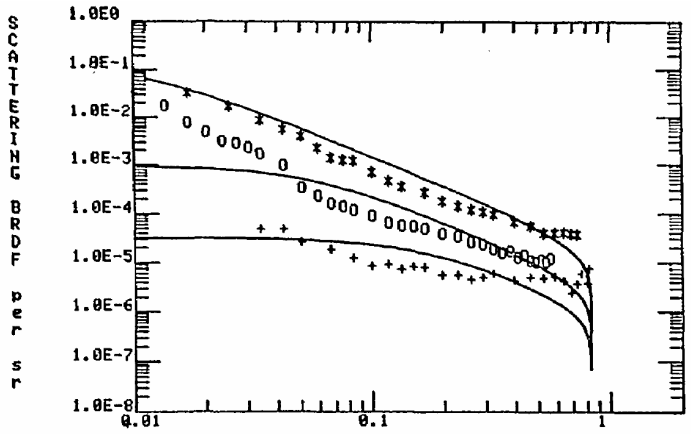

Figure 8: Wang's measurement of the BRDF for a 0.8nm Al coated mirror vs Beta (sinθ - sinθi) for 633nm (*), 3.39μm (o), and 10.6μm (+) at 10° incidence.

The coating data shown in Figure 8 above were obtained from Wang. It shows the measured BRDF for three different wavelengths for an Al-coated substrate with 0.8nm RMS roughness (via Talystep profilometer – bandwidth unspecified). A line was fit to the 633nm data above beta=0.1 and an equivalent MIST model obtained. MIST was then used to scale these data to 0 degrees incidence angle and 1075nm. The low-frequency data show a steeper slope below beta=0.1 and were disregarded as possibly being contaminated by instrument signature. As it turns out, the upward trend is compatible with a model of a 0.8nm print-through of the substrate roughness. In any case, to model the coating the data above 0.1 are most appropriate. Though we assume the Wang data are representative of coatings for COSMO, there is undeniable uncertainty here.

Figure 9 shows the results of taking the quadrature sum (blue) of the Wang BRDF data (green) and a substrate contribution modeled from a 1nm RMS roughness and a 2-D slope of 2.3 (red). Notice that the two curves cross at about 1.7 degrees – slightly larger than the FOV for a coronagraph. This implies (for the 1nm roughness shown) that the scattering will be substrate-dominated.

To calculate the scattered light level in the image plane of the coronagraph from these data, a two-dimensional integration over the solar disk is required. For every point on the solar image the limb darkening is calculated[20] as well as the angle subtended by that point and a fixed point in the coronal field of view (at the elevation of interest), with a vertex at the objective (see Figure 2). That angle is the scattering angle. Combined with the composite BRDF, the scattering contribution from each element (dA) on the disk is

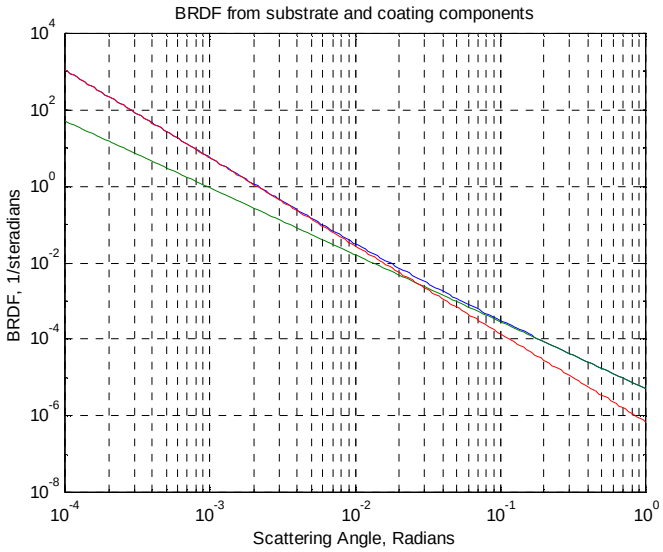

Figure 9: The net BRDF (blue) shown with the coating and substrate components

calculated and a simple numerical integration is conducted in polar coordinates (using 100 radial and angular bins, 10,000 elements total). All points on the objective are assumed to contribute equally to the scattering; the calculation is independent of aperture, f/ number, or off-axis tilting.

Figure 10 shows the result for a mirror when the integration is repeated for several elevations in the corona. A 0.7nm RMS substrate is assumed (for comparison with SOLAR-C).

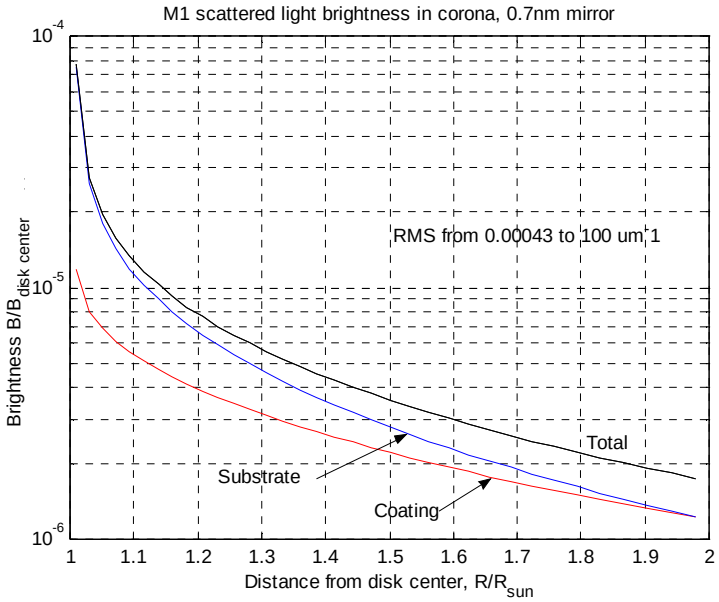

Figure 10: Predicted roughness-only scattering in the SOLAR-C telescope.

As the figure shows, 0.7nm RMS roughness is an interesting boarder-line case; the cross-over between substrate and coating contributions happens at 0.5 degrees, which is in the

middle of the scattering angles of interest. In the low corona the scattering angles are less and the scattering is dominated by substrate roughness. In the upper corona the angles are larger and the coating starts to dominate. The predicted roughness-only scattering at 1.1 radii from disk center is around 13ppm. The level actually seen in SOLAR-C at this elevation is around 20ppm, for a freshly cleaned mirror.[21] Since removing all dust isn't possible, we believe these data are nicely consistent with observed levels of scattering in SOLAR-C.

This calculation does *not* take into account the 4-10 times higher scattering that others have seen in TIS measurements of coated optics as mentioned earlier. We therefore consider these results a lower-bound.

It is important to note that unlike a substrate-only model, these results will not scale with the RMS roughness squared, until you get above approximately 1nm RMS. Below 1nm RMS, the scattering qualities of the coating become significant. These calculations show that even with a perfectly smooth substrate and no dust, the scattering at 1.1 cannot go below 5.5ppm with any Al coating technology we were able to reference.

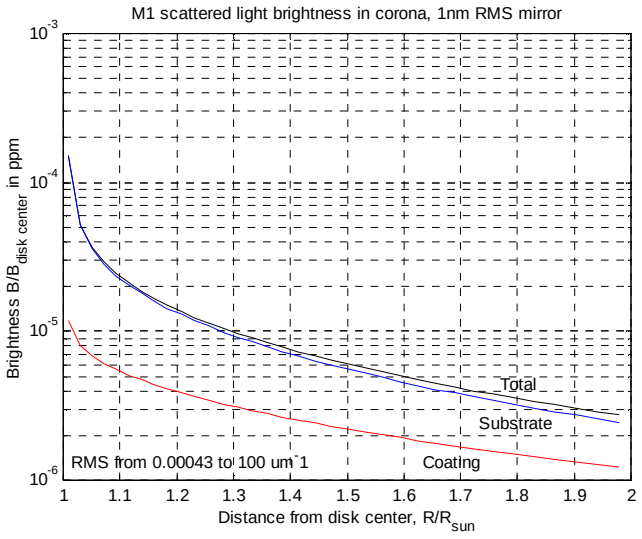

Figure 11: Roughness-only scattering for a 1nm RMS mirror.

Figure 11 shows the case for a 1nm substrate. At this point, the substrate clearly dominates. Figure 12 shows the expected levels for a 2nm RMS finish. The calculation estimates that the roughness-only scattering at 1.1 radii from disk-center is expected to be 100ppm. Note that the level of scattering from the 2nm substrate finish is totally dominated by the finishing of the substrate. The net scattering curve and the substrate-only curve are so close that they are almost indistinguishable on this plot. It is important to note that the cross-over angle between substrate and coating contributions is fairly sensitive to the modeling; the (2-D) slopes of 1.75 and 2.3 for the two components are close enough so a fairly small change in the level of one or the other can move the cross-over significantly. Although there is also significant uncertainty in whether or not the Wang data are representative of 'typical' coatings, there are two important things to consider: First, the levels shown in Figure 12 are so strongly dominated by the substrate

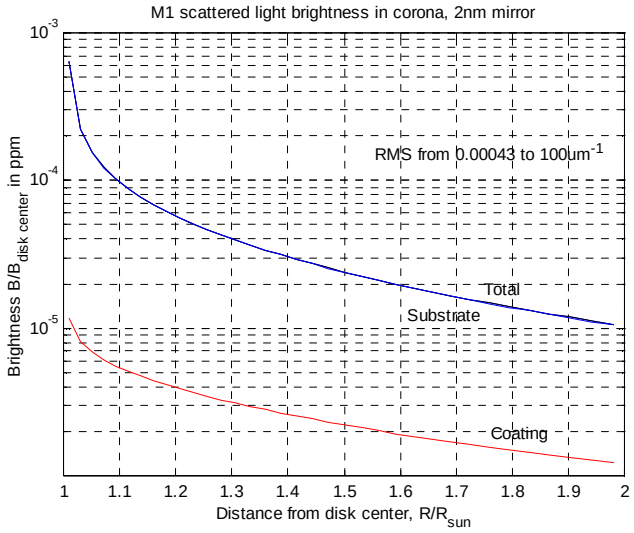

Figure 12: The predicted roughness-only scattering for the likely ATST M1 finish (2nm RMS).

that small uncertainties in the coating scattering component are insignificant. Secondly, and perhaps most importantly, is that the coating can only make things *worse;* lower levels in coating scattering will not lower the resultant curve, whereas higher levels of coating scattering can only bring it up.

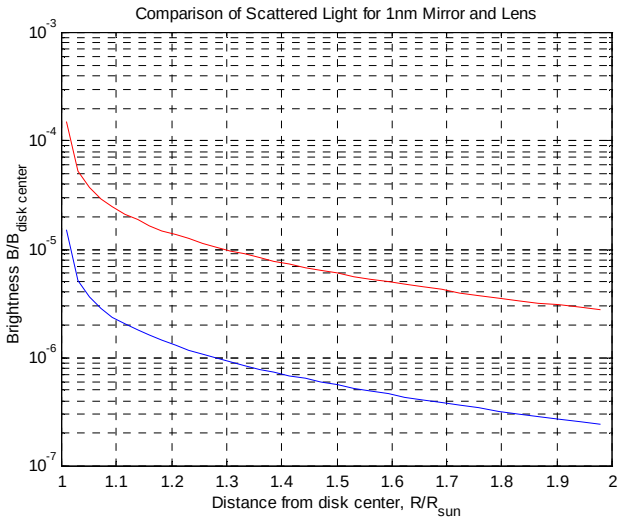

Figure 13: Comparison of 1nm RMS substrate mirror w/ Al coating (red, top) and an uncoated lens with a 1nm RMS finish on both front and back surfaces (blue, bottom).

Finally, we can compare the scattered light brightness for a mirror and a lens with the same 1nm RMS polish (Figure 13 above). The lens assumes the same polish on both surfaces. It can be scaled with the RMS roughness squared up or down, however the mirror curve can only be scaled to larger RMS values. Notice that the level of scattered light at 1.1 for the lens is nearly five times lower than the coating-only (perfect-substrate) limit for a reflector.

In summary, the two-component model for mirrors reconciles the difference in the observed scattering functions (BRDFs) from Harvey and others with the typical microroughness of substrates. It is a consistent model which reproduces most of the data we have been able to find to date[22]. While the scattering will scale like RMS roughness squared for values of 1nm or larger, the intrinsic scattering of aluminum coatings will dominate for super-smooth surfaces. Down to 1nm finishes, the quality of the coating required for solar work is 'standard'. To push levels of scattering below 10ppm, great care will have to be given to the coating. Even with perfect coatings, the refractor has a factor of 10 lower scattered light than a reflector with the same polish quality.

Dust Contamination

Figure 14 below shows the total scattered light (instrument + sky) in the Mk4 coronagraph at the Mauna Loa Solar Observatory (MLSO) for a time period of approximately 2 years. The different colored symbols represent elevations in the corona from 1.15 to 2.5 radii from disk center. The large drops in the intensity indicate dates where the objective was removed from the telescope and thoroughly cleaned. The cleaning at the beginning of 2006 was the best in this period, with the resulting scattered light at 1.15 radii of only 7ppm (3ppm at 2.5 radii).

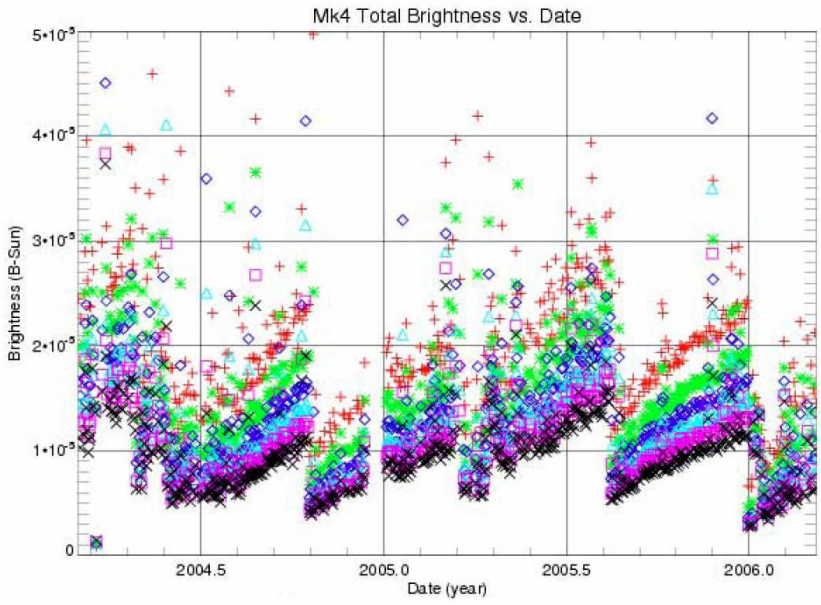

Figure 14: Scattered light from MLSO's Mk4 coronagraph

Because scattering levels are independent of telescope aperture, it is realistic to expect the same performance shown above for a large aperture telescope with COSMO (assuming the same site, equal polish quality and levels of inclusions, etc.). This gives us a powerful check for larger telescopes – particularly refractors. Unfortunately there are relatively few internally-occulted reflecting coronagraphs and their data sets are relatively sparse, making such checks much more difficult.

Figure 14 directly demonstrates that dust contamination is the dominant source of scattered light. If microroughness, inclusions, or other stationary sources of scattered

light were significant, one would expect the level of scattering to remain constant for a while after a cleaning. As the contamination level increased, the scattering would eventually start to increase. That is not what these data show. It is clear that the scattering increases from the first day after cleaning, and therefore dust is the dominant factor. It is important to note that the Mk4 coronagraph is located on Mauna Loa, HI on a 1935 lava flow. There is no vegetation for tens of km, making it one of the 'cleanest' observatories in the world. The Mk4 lens is more than 25 years old, and is blown off with an air gun every morning to remove larger pieces of detritus. With daily air dusting, the rate of scatter increases by approximately 19ppm/year.

Modeling Dust

Dust is typically modeled as dielectric spheres, the scattering from which can be calculated using Mie scattering theory. As Figure 15 below shows, the forward-scattering peak (due to diffraction around the particles) grows in height as the 4th power of the diameter. Since the highest angle of interest in scattering for a coronagraph with a 1º FOV is 0.75º, the strong forward scattering by larger particles dominates. Rayleigh scattering only applies for particles much smaller than the wavelength and is insignificant compared with the Mie scatterers.

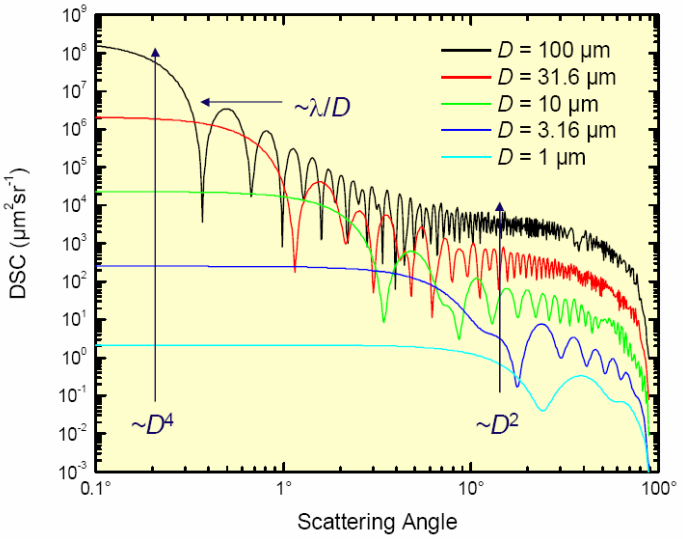

Figure 15: Scattering by particles on a lens as calculated by Mie theory (courtesy of Thomas Germer, NIST Optical Technology Division).

Figure 15 shows the Differential Scattering Cross-section (DSC) for different sized dielectric spheres. The DSC can be converted into a BSDF for calculating the scattering in a telescope if there is a distribution model for the number of particles per unit area on the objective. The 'standard' distribution is the MIL-STD 1246C:

$$N(D) = 10^{0.926\left[(Log_{10}Xc)^2 - (Log_{10}D)^2\right] - 10.968} \quad \mu m^{-2} \qquad [1]$$

For a given cleanliness class (X_c), the quantity N(D) describes the total number of particles of diameter (D) and larger. The minimum diameter of particle in the 1246C standard is defined at 1µm, and the largest diameter is equal to the cleanliness class (in a

X_c=200 distribution, the largest particle present is 200μm). Though sometimes criticized as not representing real distributions, it is the most widely cited standard and the one we adopt here. Figure 16 below shows the fractional area coverage of a mirror vs the 1246C cleanliness class. An ATST technical report[1] notes that carefully cleaned surfaces have around 10^{-4} area coverage, corresponding to a 1246C class of 239.

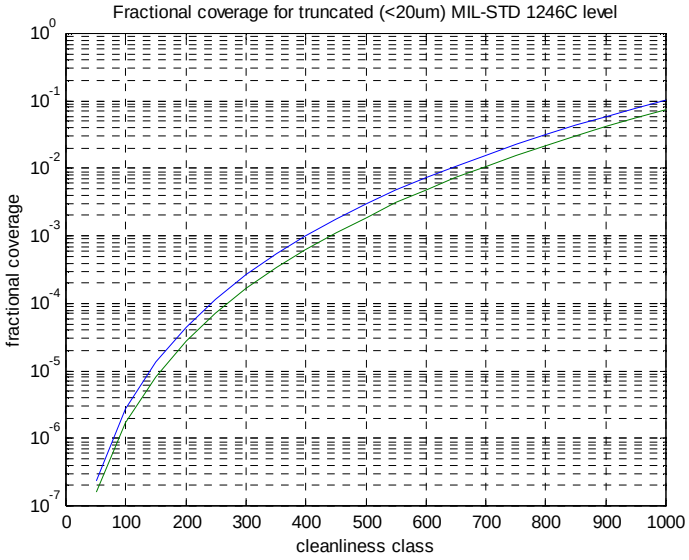

Figure 16: Fraction area coverage for normal MIL-STD 1246C distribution (blue) and with all particles larger than 20μm removed (green).

The green curve in Figure 16 indicates the fractional coverage when the 1246C distribution is truncated by eliminating all particles above 20μm in diameter. This is done to approximate how the distribution might change when a lens is dusted with an air gun. Due to the steep slope of the 1246C distribution, the fractional coverage is strongly dominated by the particles in the 1-20μm range.

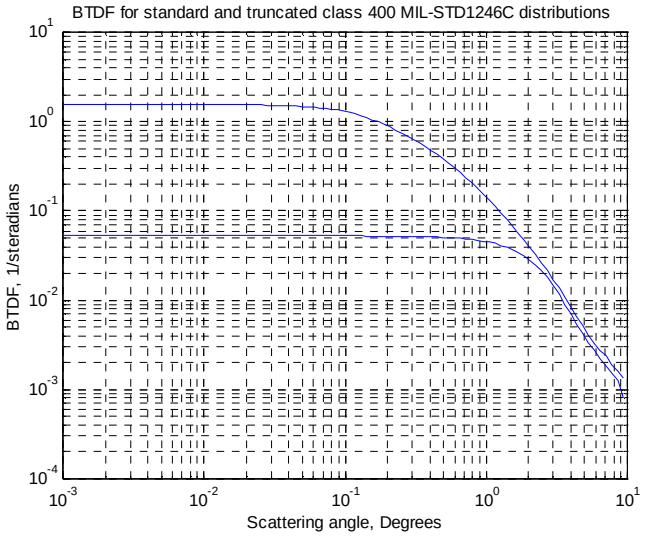

Figure 17: BTDF for a standard and truncated (<20μm) class 400 MIL-STD1246C distribution

The MIST modeling software can be used to calculate the BSDF for the scattering from a range of particles with densities defined by MIL-STD1246C. In this case, we start with the minimum 1μm diameter and increment it by a factor of 1.1 up to the largest diameter. Adding those BSDF together (assuming linear superposition) gives us the net BSDF for the distribution. Figure 17 shows the result for a standard class 400 surface (top curve), and for the truncated (<20μm) distribution shown in Figure 16. Note that truncating the distribution moves the knee to higher scattering angles. This simply reflects the fact that larger particles are more sharply peaked in the forward direction. The truncation has lowered the low-angle BSDF dramatically. These data can be integrated in an identical manner to the microroughness BSDFs to produce the expected level of scattered light in the coronagraph. Figure 18 shows the results for a lens with class 400 contamination (both standard and 20μm-truncated) compared with the level expected for a 1nm RMS surface roughness:

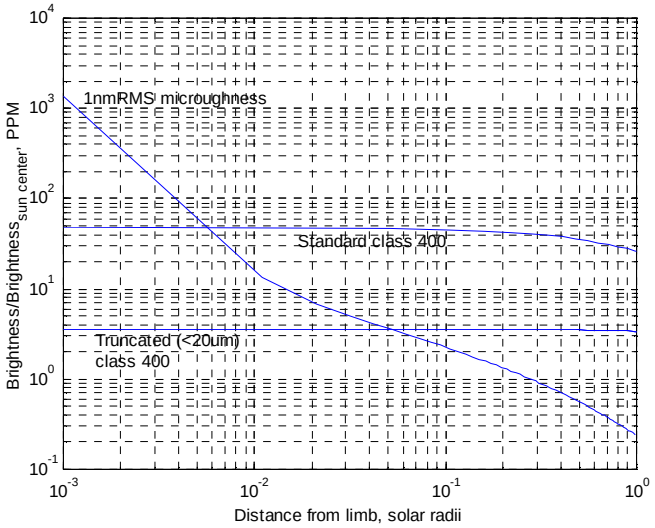

Figure 18: Comparison of scattering due to 1nm RMS microroughness with standard & truncated (<20μm) class 400 MIL-STD1246C contamination (for a lens).

As expected, the contamination dominates at elevations of 0.1 radii above the limb and higher. Microroughness, however, could dominate scattered light at lower elevations due to its steep slope. Note the scattering from dust is almost flat across the FOV. Figure 15 shows that the scatter decreases by about a factor of 2 between 1.15 and 2.5 radii. This is more consistent with the standard distribution than the truncated one. Note the truncated distribution produces a factor of 10 less scatter. This is perhaps un-intuitive, since Figure 16 shows the removed particles are a tiny fraction of the total area covered. This simply reflects the (diameter)^4 dependence on the forward-scattering peak.

Accumulation rates have been measured at Mauna Kea, HI in the UKIRT telescope by measuring the emissivity of witness surfaces as a function of time. Those data are shown in Figure 19[1]. It is very difficult to reconcile this accumulation rate with the Mk4 data shown in Figure 14. To reasonably model the Mauna Loa data (assuming air cleaning removes all dust larger than 20μm) an accumulation rate at least 15 times lower (0.000072%/hour) is required. This is probably reasonable; as mentioned, the MLSO site

is very clean. In addition, the MLSO facility is dedicated with virtually no human activity in the dome. The Mk4's objective is protected by a cover except when the telescope and dome are ready to observe, and the objective is constantly washed in HEPA-filtered air. The lava fields at Mauna Kea are much older with lots of dusty soil, the UKIRT objective in an open-structure telescope deep inside the dome, and the dome sees a much higher level of human activity.

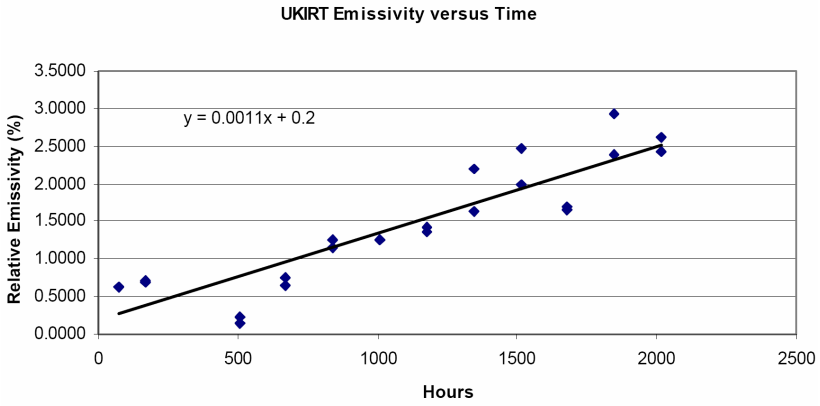

Figure 19: Emissivity of test plates vs time for the UKIRT telescope show a particle accumulation rate of approximately 0.0011 percent (area) per hour

With the MIL-STD 1246C distribution and the accumulation rates inferred from the MLSO Mk4 data, we can calculate the expected scattering in the telescope as a function of time. The lens calculation assumes two surfaces of equal initial contamination, and ages only the surface exposed to the outside environment. The mirror calculation assumes a "double-interaction" model where the effects of the particles' mirror image is considered. Those results are shown below.

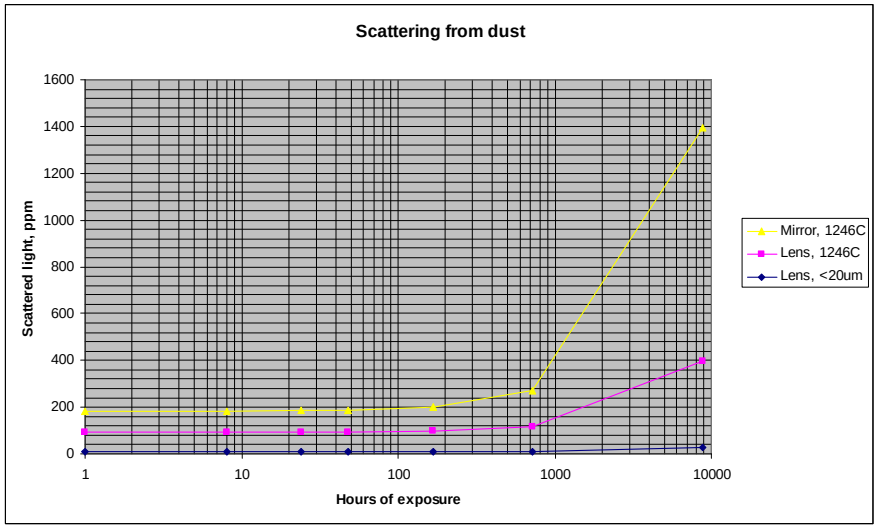

Figure 20: Scattering at 1.1 radii from MIL-STD 1246C distribution.

The lowest curve in Figure 20 is shown only for reference; it matches the measured rates of the Mk4 data (assuming a 0.000072%/hour accumulation rate, 0.001 initial fractional coverage, and a 20μm-truncated distribution). Note that dusting reduces the scattering by

more than a factor of 10. Air-cleaned data for reflectors is not shown since it has not been demonstrated that aluminized coatings can withstand such long-term daily treatments.

Most relevant are the top two curves (yellow and purple). They show that for equal contamination levels the mirror-based telescope produces 4 times more scattered light than a lens-based design. This turns out to be a general rule: the DSC for a single particle on a mirror produces 4 times higher scattering than the same particle on a lens, approximately independent of the particle's size. By linear superposition, any distribution of particles produces the same factor of 4 difference.

Based on these data, we conclude that a reflecting telescope would need double the aperture to achieve the same S/N ratio of a refractor in the noise-dominated regime[23].

Dust Control

The current concept for both designs is to "flush" the objective with clean air. For a reflecting design the entire optical path would be closed with only the entrance aperture open to the outside environment. HEPA-filtered air would wash over the mirror (to help control its temperature), and leave the telescope through the aperture. The volume of the air would be relatively large to ensure adequate velocity to prevent dust from entering the telescope through the aperture. The air would be temperature controlled to minimize seeing as the air leaves the telescope. Since COSMO is almost a factor of 5 from diffraction limited (due to its wide FOV) seeing is less critical than in telescopes such as ATST.

To implement this strategy for a refractor, a 'snorkel' must be put on the end of the telescope tube. For the outward flow to be uniform over the aperture, this snorkel should be 2-3 times the aperture diameter in length. We envision this snorkel as a tube which is extended through the dome slot, thus preventing the need for a larger dome. The tube would probably contain air plenums and also hold the main lens cover. The reflector clearly has an advantage in avoiding these mechanical complications because the tube acts like a snorkel.

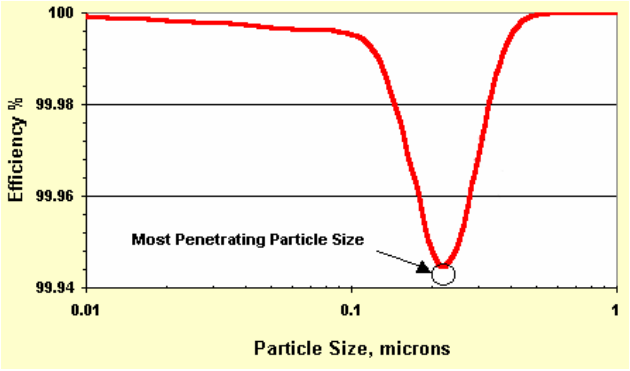

Figure 21: Efficiency of HEPA filters vs particle diameter.

Figure 21 above shows filtering efficiency of standard HEPA filters. Note that above 0.3 microns the efficiency is in excess of 99.99%. The "most penetrating particle size" of

0.25 microns is of little consequence since particles of that size produce almost no scattered light. The air filtering system would remain powered 24/7/365 even when the telescope is covered and stowed to provide "positive pressurizing." Such filtering may eliminate the need for 'air cleaning' the objective. This is particularly important for a reflector, for which direct cleaning of the mirrored primary is expected to be problematic. Modeling an air washing system is difficult. Evaluating this scheme's actual effectiveness will require computational fluid dynamics simulations or building a prototype. As mentioned, the MLSO Mk4 objective is washed with HEPA-filtered air, however the Mk4 does not use an extended snorkel as we propose here.

Cleaning

Even with an air flushing system, it is likely that the objective will require regular cleaning. Refracting coronagraphs have proven durable under regular cleaning for decades. Careful procedures combined with the inherent hardness of glass make cleaning lenses safe. This is clearly a major advantage for refractors given the fact that contamination dominates telescope performance.

Cleaning is a major problem for reflectors. Aluminum is much softer than many of the contaminants we expect, such as volcanic rock dust. Removing such particles inevitably degrades the quality of an aluminum coating. Frequent re-coating of the mirror may be required. Another option is to use a protected silver coating which would both reduce mirror seeing (by reducing heating) and improve the cleanability of the mirror. The drawback of this is a much more difficult stripping and coating process.

A related concern is the durability of the objective under exposure to unexpected weather. This includes sudden rain storms or accidental exposure to condensation conditions. Direct exposure to moisture will demand cleaning the objective. It is unclear whether a mirror can be cleaned after exposure to liquid water without re-coating.

Inclusions (refractors only)

Historically coronagraph lenses have been made as thin as possible. One of the main reasons was to reduce the total number of inclusions in the bulk of the glass. Inclusions are primarily trapped air bubbles, but may also include such things as pieces of metal (typically platinum from the walls of the melt tank) and solid impurities from the raw material. Like particulate contamination on the surface, inclusions scatter light. Unlike most common dust, some of the inclusions can be very large; air bubbles can be up to 1mm in diameter in some materials. As before, MIST is used to calculate the DSC for an air bubble inclusion in a fused silica substrate. Figure 22 shows the scattered light contribution at 0.1 radii above the solar limb for a single inclusion vs inclusion diameter. This calculation assumes a 1.5m aperture. The scatter from a single inclusion is independent of the aperture, but the image brightness is not. As a result, this calculation needs to be scaled for apertures other than 1.5m.

Note that these data are valid at almost all elevations, since Figure 18 shows the scattering from particles is nearly flat across the entire FOV. If the goal is to have less than 1ppm total scattering from inclusions, the data above show that we could tolerate

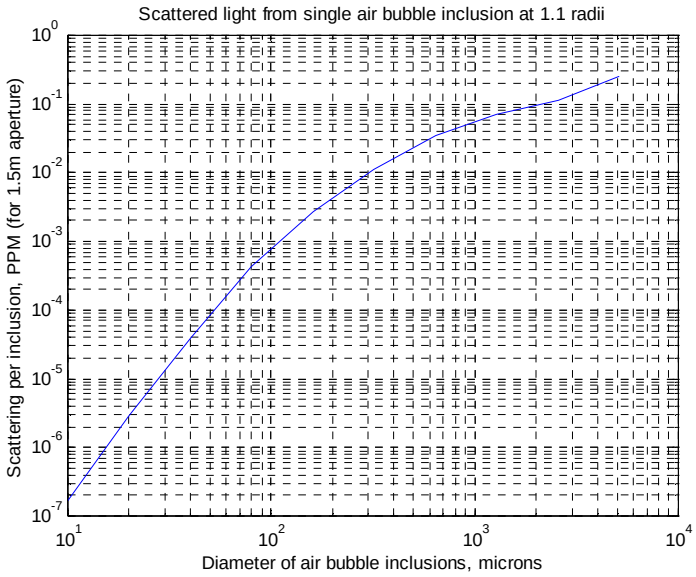

Figure 22: Scattering due to air bubble inclusions in fused silica.

only ten inclusions of 2mm diameter in the 425kg of glass which make up the 1.5m lens. We can tolerate 100 inclusions of 0.3mm diameter, 1,000 inclusions of 0.1mm diameter, or 10,000 inclusions of 0.05mm diameter and so on.

Fortunately, the telecommunications industry has driven the development of high-purity fused silica. A standard-grade Corning 7980 blank of the needed size is likely to yield a blank with less then 20 inclusions ranging from 0.10mm - 0.25mm diameter. Corning 7980 is not tank-melted, and thus does not contain metallic contaminants. It is made in what is essentially a massive deposition process called "flame hydrolysis": silicon tetrachloride gas is oxidized by reaction with water (H_2O) in an oxyhydrogen flame and the resulting 'soot' is accumulated. All inclusions are gaseous, and typically round. At the levels quoted from Corning, inclusions are not expected to be an issue.

Rayleigh Scattering (refractors only)

An important loss factor for optical fibers is scattering from impurities. These have been reduced to such a low level in fused silica that the dominant loss is Rayleigh scattering. The level of Rayleigh scattering for several glasses has been measured by Germer, and is shown in Figure 23 below. (σ) represents the fractional loss per cm of glass. The scattering drops off faster than $1/\lambda^4$ because there is also an index of refraction dependence in the scattering[24]. The level of scattering loss from Rayleigh scattering at IR wavelengths is ~0.3dB/km of glass! Though significant for optical fibers, this is incredibly low by historical standards. After extrapolating these data to 1075nm, one can calculate that the scattered light contribution at 1.1 radii is on the order of $5x10^{-11}$. It is not an issue.

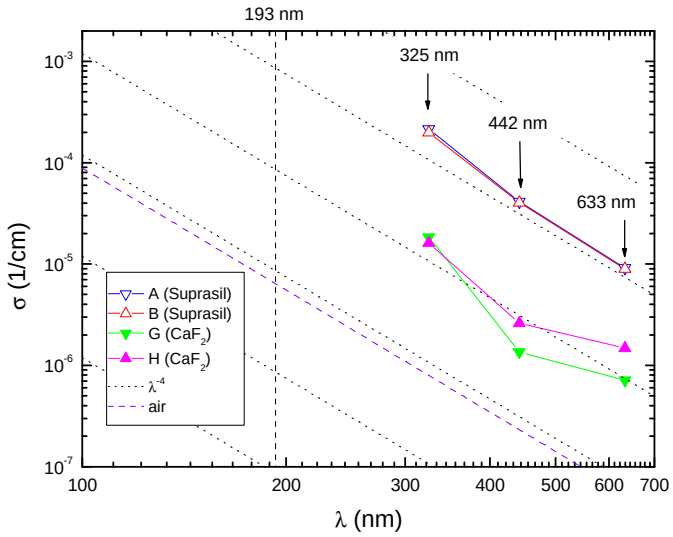

Figure 23: Meausred Rayleigh scattering for fused silica (Suprasil)

Index variations (refractors only)

All glasses have inhomogeneities in their index. Figure 24 shows the measured index variation for the central 600mm region of a 1524x200mm 7980 fused silica boule. The central region is the worst part of the boule, but is still under 3.3ppm in homogeneity. The measurement was made with a 24" Zygo interferometer at 633nm. Except for a sharp peak at the boule's center, all of the variations are at low spatial wavelengths.

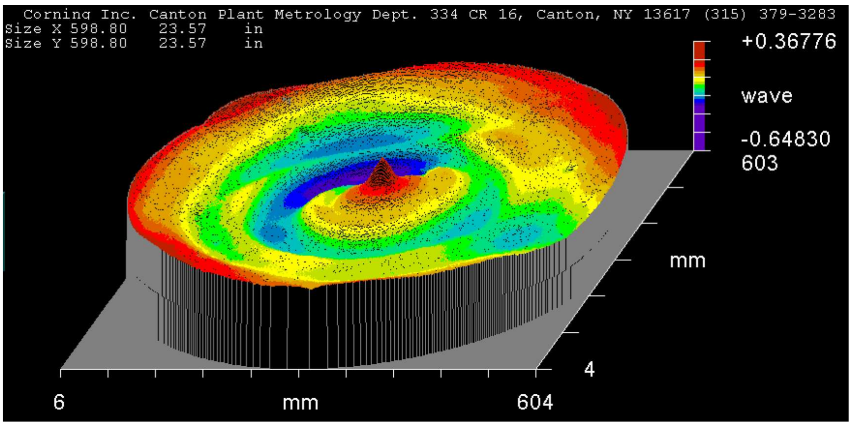

Figure 24: Measured homogeneity of the center 24" area of a 1524x200mm Corning 7980 Boule.

These long-wavelength variations have been modeled as a gradient-index model in Zemax optical modeling software. Since Zemax is not capable of applying an index gradient to an aspherical optic, the geometry had to be modified. A spherical optic of the same size as the real objective (to within the 20μm aspheric correction) is combined with

a double-asphere to correct aberrations (Figure 25). Zemax supports 7th order polynomials even in (R) to describe an index. We experimented with a wide variety of profiles, two of which are shown in Figure 26. The amplitudes of the variations were normalized to match the peak index variation from the Zygo data. Note that sharp features like the central bump in the boule are difficult to model with a 7th order polynomial. Fortunately, the central 10mm of the boule is the only part showing 'sharp' variations. If this cannot be removed with local polishing, a larger than normal Lyot spot could block its influence (10mm being a negligible fraction of the aperture's area).

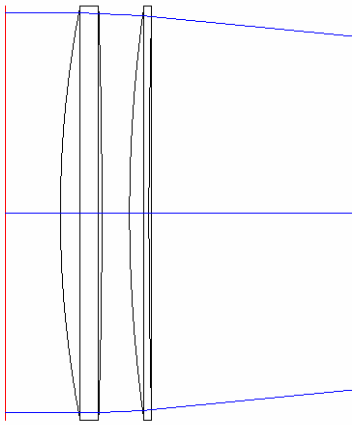

Figure 25: Zemax model for estimating effects of index inhomegeneities

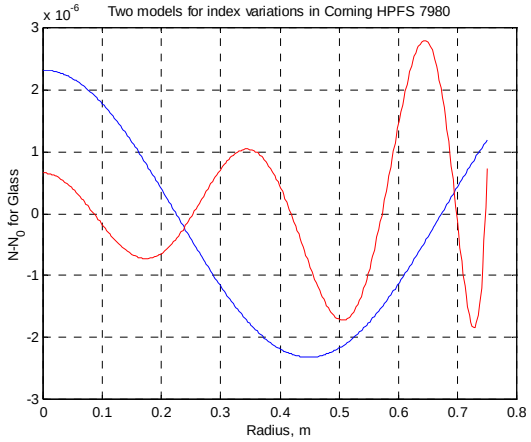

Figure 26: Two models for index variations based on 7th order even polynomial in R

The spot diagrams (at the edge of the limb) as calculated by Zemax are shown in Figure 27. In the figure, the box represents the size of a camera pixel (assuming 4096x4096 coverage of a 1º FOV), and the circle represents the Airy disk. The nominal spot diagram (a) has a different shape than in the nominal (single-lens) design, but is close enough for these purposes. (b) shows the spot diagram for the index shown in blue in Figure 26. This is considered a realistic model for the index variations. The red curve in Figure 26 represents the most extreme model which we could construct with a 7th order polynomial. (c) shows the corresponding spot diagram. Though it is larger than the camera pixel, the RMS size of the spot is still small compared with the pixel. Note that all of these variations will probably be corrected in the polishing of the optic. Zemax can also

perform a FFT analysis of the point spread function (PSF) which takes into account the coherent interference of the rays passing though the lens. As expected, the PSF is broadened by the variations, but no significant increase in the wings of the PSF are observed. Thus, index variations are not expected to be an issue.

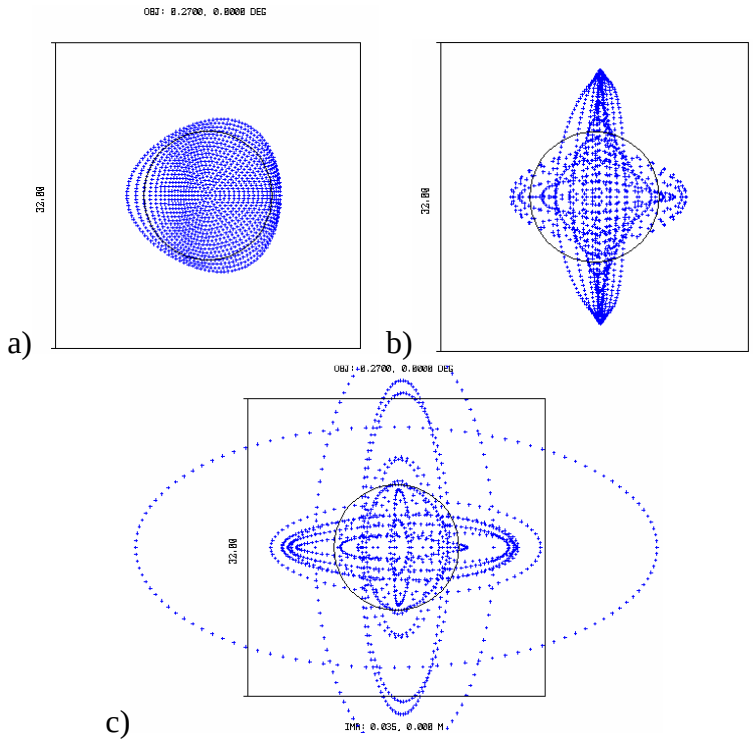

Figure 27: Spot diagrams for a) uniform index, b) likely index variations, and c) extreme model

Striae (refractors only)

A special class of index variations are called striae shown in a 'shadowgraph' picture below.

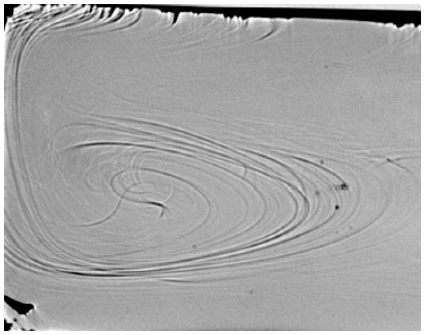

Figure 28: Striae in a standard optical glass like BK-7 (a sample which failed QC).

Striae are typically formed by a combination of incomplete mixing of materials in a melt tank, and convective currents which are then frozen when the melt cools. They usually have a sheet-like topology which causes large phase distortion when viewed edge-on, but almost none when viewed normally to the sheet. They are of particular concern because

their spatial scale is a few mm to cm, which is exactly the spatial scale required to scatter into the angles of interest in a coronagraph. In general, smaller blanks allow better mixing and have lower levels of striae. This is another reason coronagraph lenses made from traditional glasses have been as thin as possible.

Fortunately, high-purity fused silica is not made by mixing components in a melt tank, but is deposited in layers from a single-component, extremely pure gas. What variations are caused by the layering in the 'deposition' process tend to be perpendicular to the optical axis of the blank. Corning has represented to us that 7980 has "no striae". They are not expected to be a problem with fused silica glass.

Conclusion

We have examined all known potential sources of scattering at the objective of both reflecting and refracting coronagraphs. The dominant source at 0.1 radii from the limb and above is dust. Reflectors produce 4 times more scattered light than refractors for equivalent levels of contamination. Reflectors present serious issues when cleaning the primary is considered, whereas refractors have a proven record of cleanability to adequate levels. At low elevations in the corona, microroughness could dominate. For this source, refractors have a 10 times better performance than reflectors given a perfect mirror coating. There is ample literature to suggest that scattering in reflectors will be dominated by point defects in the coating, which could increase the scatter by a factor of 3 or more over the microroughness values. Scattering from imperfections in the bulk of the refractor's glass lens has been mitigated by the availability of ultra-high purity fused silica developed for the telecommunications industry. These seem negligible compared to contamination and microroughness.

---

[1] Hubbard, R., "M1 Microroughness and Dust Contamination, " Advanced Technology Solar Telescope Technical Nove No.0013, Rev. C

[2] Stover, J. C., et. al., "Comparison of surface PSD's calculated from both AFM profiles and scatter data," (SPIE **3275**, 37-46, April 1998)

[3] Walch, C. J., et. al.,"Fabrication and Measurement of Optics for the Laser Interferometer Gravitational Wave Observatory," (Applied Optics **38**, No. 13, 1 May 1999.)

[4] Stover, John C., *Optical Scattering – Measurement and Analysis*, SPIE Press, 1995, Bellingham, WA, 2nd ed. 1995.

[5] Germer, T.A., "Predicting, Modeling, and Interpreting Light Scattered by Surfaces," presentation given as SPIE Short Course SC492, Feb. 2002

[6] Church, E.L., "Fractal Surface Finish," (Applied Optics **27**, No. 8, 15 April 1998.)

[7] Duparre, et. al., "Surface characterization techniques for determining the root-mean-square roughness and power spectral densities of optical components," (Applied Optics **41**, No. 1, 1 January 2002.)

[8] Newkirk G., and Bohlin D., "Reduction of Scattered Light in the Coronagraph," (Applied Optics **2**, No.2, 131-140, February 1963.)

[9] Hickman, K.C., et. al., "Correlation between substrate preparation technique and scatter observed from optical coatings," (Applied Optics **32**, No.19, 3409-3415, July 1993.)

[10] Bennett, J.M., et. al., "Relation between optical scattering, microstructure and topography of thin silver films. 1: Optical scattering and topology" (Applied Optics **24**, No.16, 2701-2711, August 1985.)

[11] Thomas Germer, Optical Technology Division of the National Institute of Standards, Gaithersberg, MD., private communication.

[12] Wang, Y., and Wolfe, W., "Scattering from microrough surfaces: comparison of theory and experiment," (J. Opt. Soc. Am. **73**, No.11, 1596-1602, November 1983.)

[13] Korendyke, C.M., "Measurement of near-specular visible-wavelength scattered light from two superpolished "coronagraph quality" mirrors,"
[14] Hyun-Ju, C., et. al., "Effects of substrate and deposition method onto the mirror scattering," (Applied Optics **45**, No.7, 1440-1446, March 2006.)
[15] Guenther, K.H., et. al., "Surface roughness measurements of low-scatter mirrors and roughness standards," (Applied Optics **23**, No.21, 3820-3836, November 1984.)
[16] Kiesel, A., et. al., "Surface Finish Assessment of Synthetic Quartz Glass," (SPIE **2775**, 140-146, 1996)
[17] Duparré, A., et. al., "Multi-type surface and thin film characterization using light scattering, scanning force microscopy, and white light interferometry," (SPIE **CR72**, 213-231, July 1999.)
[18] Robert Hubbard, National Solar Observatory, private communication.
[19] Wuttig, A., et.al., "Surface roughness and subsurface damage characterization of fused silica substrates," (SPIE **3739**, 369-375, May 1999.)
[20] Neckel, H., "Solar Limb Darkening 1986-1990 (λ 303 to 1099nm)," (Solar Physics **153**, 91-114, 1994,) and "Analytical Reference Functions F(λ) For The Sun's Limg Darkening And Its Absolute Continuum Intensities (λ 303 to 1100nm)," (Solar Physics **229**, 13-33, 2005.)
[21] Haosheng Lin, Institute for Astronomy, HI. Private communication.
[22] Many of the references are in conflict, so complete reconciliation is impossible.
[23] Tomczyk, Steven, "COSMO Error Estimates," COSMO Technical Note No. 1, Sept. 2006
[24] M.E. Lines, J., "Scattering losses in optic fiber materials. I - A new parameterization. II - Numerical estimates," Appl. Phys. **55**, 4052-4063 (June 1984).